Analysis of output precision characteristics of digital switching power amplifier in the active magnetic bearings system

Xin Cheng, Lin Zhang, Rougang Zhou, Shao Song, Bo Wang & Han Liu

Published online: 15 Nov 2017.

Submit your article to this journal

Article views: 413

View related articles

View Crossmark data

Citing articles: 5 View citing articles

Analysis of output precision characteristics of digital switching power amplifier in the active magnetic bearings system

Xin Cheng[a,b]*, Lin Zhang[a], Rougang Zhou[c]*, Shao Song[d], Bo Wang[a] and Han Liu[a]

[a]School of Mechanical & Electronic Engineering, Wuhan University of Technology, Wuhan, Hubei, China; [b]Hubei Maglev Engineering Technology Research Center, Wuhan University of Technology, Wuhan, Hubei, China; [c]School of Mechanical Engineering, Huazhong University of Technology, Wuhan, Hubei, China; [d]China Ship Development and Design Center, Wuhan, Hubei, China

ABSTRACT

Power amplifier is the key component of the magnetic bearing systems, and its precision characteristics have decisive influence on the overall performance. We analyze the factors in the formation of precision characteristics of typical digital switching power amplifier under two-level modulation, and reveal that the inherent ripple characteristic and precision of current detection are the main limits. The relationships between inherent ripple characteristic and its main influencing factors, such as bus voltage, modulation frequency and constants of electromagnetic coil have been derived in this paper. By suppressing the analog noises and drifts in current detection circuit, and calibrating the analog to digital converter, the precision performances of the current detection circuit had been improved efficiently to avoid becoming the dominant factor of the formation of the precision characteristics, which make that the precision of output current is nearly determined by the inherent ripple characteristic. The experimental results show that the output current ripple is very close to the inherent ripple characteristic if the precision of current detection circuit is high enough. Furthermore, the approaches discussed can describe the formation of precision characteristics by theoretical calculation of inherent ripple characteristic under the conditions of different implementations.

1. Introduction

Magnetic-levitated actuators, with the advantages of no mechanical contact, no wear, no lubrication and controllable bearing characteristics, are the crucial components of the equipment, such as turbine machine, vacuum pump, high-end manufacturing facilities and attitude control gyroscope of spacecraft [1,2]. The common forms of magnetic-levitated actuators are MLPAs (magnetic-levitated planar actuators) [1,3,4], widely used in 6 degrees-of-freedom (DOF) ultra-precision stage [5–8] for planar motion, while the magnetic bearings are the other forms of magnetic-levitated actuators for rotational motion application.

Power amplifier (PA) is the energy conversion part of an active magnetic-levitated system, which provides the desired current in the electromagnetic coil to generate the desired electromagnetic forces. Precision characteristics are the crucial performance indicators of PA [2]. The insufficient precision of PA will increase the nonlinearity in the magnetic bearing system [2], and meanwhile cause the unbalanced electromagnetic force and the mechanical vibration of the rotor, resulting in instability of the high-speed rotor which will be out of the controllable range [2,4].

PA in magnetic bearing system can be regarded as the current tracking control system, and DSPA (digital switching power amplifier) is the most common form. Compared with analog control, the digital control provides many advantages, such as the ability to decrease the disturbances in the analog signals, and to operate more complex arithmetic, more robustness against aging and environment variation [9]. However, digital control results in inherent time delays simultaneously, and the too large phase shift even endangers the system stability [9]. Furthermore, the nonlinear factors, such as pulse width modulation (PWM), switching and delay in power devices, and noise and drift in analog devices, make it difficult to establish an accurate model of DSPA.

Some control strategies, e.g. dead beat control [10,11], predictive control [12,13], and repetitive control [14,15] have been proposed to compensate the delays in digital close loop, and nearly achieve zero current error in theory [9]. However, the control strategies above are sensitive to system parameter variations, which means that the uncertainty in model will cause the uncertainty in output performance, endangering the overall stability, especially for the systems with redundant supporting structures [16,17].

CONTACT Xin Cheng ✉ chengx@whut.edu.cn
*These authors contributed equally to this work.

The precision characteristics of DSPA can be affected by many factors, such as bus voltage, coil constant, modulation frequency, sampling rate, and coefficients in current controller, and some modelling approaches have been proposed to help to analyze them. The electromagnetic force can be linearized when the position error of rotor is maintained in a relatively small range, wherein the DSPA can be equivalent to proportional component [18]. Or according to the approximate relationship between input and output, we can simplify the PA system to an equivalent mathematical model [19]. These kinds of simplified model can only approximately describe the output characteristics of the PA, and can be used in some robust methods [20], which can be more tolerant to the model uncertainty or error. Overall, the efforts of the controller can maintain the current tracking error in a reasonable range, and a relatively accurate model or advanced control strategies can help to improve the tracking error. However, even when the tracking error in controller is 1 digital LSB (least significant bit), the actual current error still exists, and can be affected by the errors from the current detection circuit and modulation.

Therefore, the theoretical approaches at present are not accurate enough to describe the precision characteristics of the DSPA. In this paper, we analyze the formation of the precision characteristics of DSPA, and then discuss the influence mechanism of main factors to the precision of output current. Finally, we establish an experimental platform to verify the accuracy of the approach proposed in this paper.

2. Influencing factors of the precision characteristics of the DSPA

Precision characteristics of the DSPA are described through the ripple ΔI, and drift I_b of the output current. The former refers to the high-order harmonic components in the output current, while the latter refers to drift value between the actual value and desired value, as shown in Figure 1.

Block diagram of the DSPA in magnetic bearing is shown in Figure 2, and a half-bridge structure is usually adapted to generate a unidirectional current. The commands to DSPA come from the upper position controller, while $e(t)$ is the error between the values of
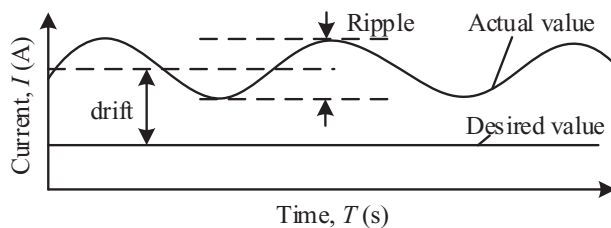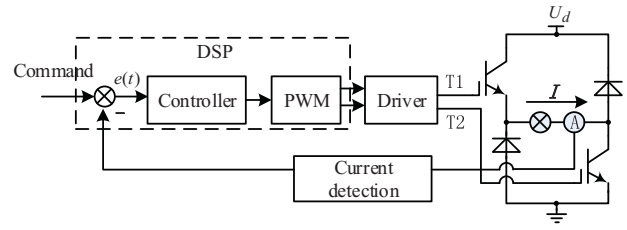

Figure 2. Block diagram of DSPA.

the command and the feedback. The operation of controller, realized in DSP (digital signal processor), will output the result to control the duty ratio of PWM module. T_1 and T_2, respectively, drive the upper and lower sides of the power bridge, with the duty ratio implied in them controlling the change of current in the load coil, and providing the output of the controlled current.

From Figure 2, the controller will try to decrease the error $e(t)$ to make the output current can follow the command under the effects of feedback control. Neglecting the small precision loss caused by digital signal processing, the other influencing factors of precision characteristics of DSPA in the actual implementation can be expressed as three types:

(1) *The error e(t) of control loop*. The range of $e(t)$ depends on the control strategies and the coefficients. Although the nonlinearities and model uncertainty exist, we still can maintain the steady state $e(t)$ as the LSB equivalent.
(2) *Inherent ripple characteristic*. This Inherent characteristic is the fluctuation of the output current caused by the bus voltage in each switching period, and mainly decided by the switching frequency, the topology of the power circuit, and the time constant of electromagnetic coil in the magnetic system.
(3) *Precision loss caused by current detection circuit*. The current detection of DPSA includes current sensor, operation amplifiers and relevant circuits. The noise and offset will affect the precision of current detection. The noise in the current detection circuit will be added to the output current ripple ΔI, while the offset will affect the drift I_b.

3. Formation of the precision characteristics

Formation of the precision characteristics of the DSPA depends on the interaction of the three types of factor in Section 2, as shown in formula (1).

$$\Delta i \approx \sqrt{\Delta i_{inherent}^2 + \Delta i_{ctrl\_err}^2 + \Delta i_{det\_err}^2}, \quad (1)$$

where $\Delta i_{inherent}$, Δi_{ctrl_err} and Δi_{det_err} are, respectively, the output current ripple components caused by inherent ripple characteristic, error in control loop and error

Figure 1. The ripple and drift of output current of DSPA.

in the current detection circuit. In the actual application, we found that if we can maintain both the errors in control loop and current detection circuit below a relatively lower value (for example, 1% of the value of inherent ripple characteristic), the total output current ripple will be very close to the inherent ripple characteristic, as in formula (2).

$$\Delta i \approx \Delta i_{inherent} \sqrt{1^2 + 0.01^2 + 0.01^2} \approx \Delta i_{inherent}. \quad (2)$$

We can develop the design approaches as follows:

(1) Based on the inherent ripple characteristic of DSPA, building the power circuit architecture, including the topology, bus voltage and switching frequency, etc., according to the desired output current precision.
(2) With the constraint of the 1% of the inherent ripple value, designing the current detection circuits.
(3) Selecting the proper controller coefficients to make the $e(t)$ within a limited range.

The above ideas make the errors in control loop and current detection circuit not become the dominant factors of the formation of precision characteristics, and therefore, we can use the inherent characteristics to describe the output precision of DSPA nearly. The key points of the above ideas are: (1) the impact of multiple factors on the inherent characteristics; (2) analysis of relationship between formation of overall output precision and accuracy in current detection.

3.1. Inherent ripple characteristic

Now we analyze the inherent ripple characteristic according to the specific topology structure of the power circuit, as shown in Figure 3.

Q_1, Q_2 and D_1, D_2 are the switch tubes and the freewheeling diodes, respectively. The electromagnetic coil is equivalent to resistor r and inductance L. Under two-level modulation, the bridge drive signals T_1 and
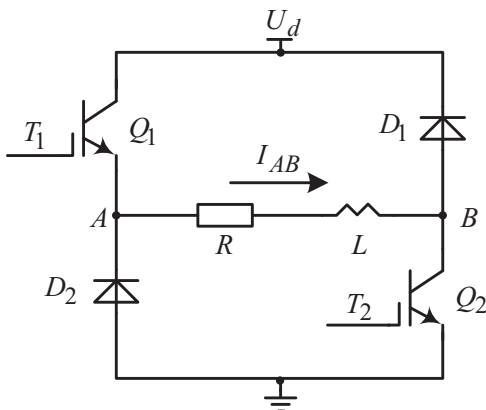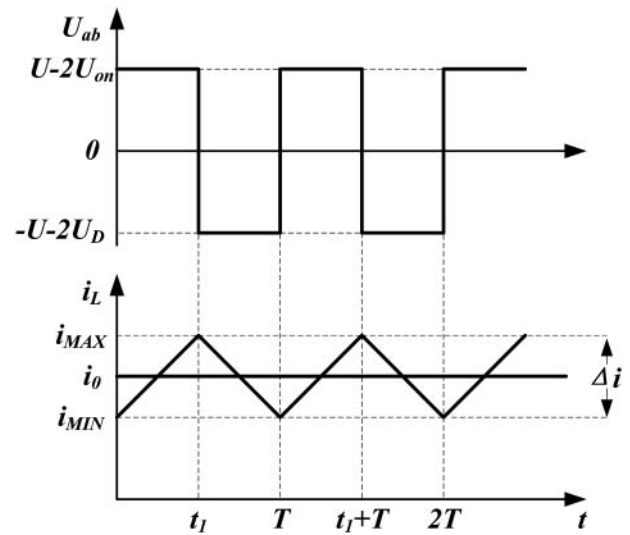

Figure 3. Power circuit in DSPA.

Figure 4. Voltage and current waveforms in 50% duty ratio under two-level modulation.

T_2 will be enabled simultaneously, making the U_{AB} switched between U_d and $-U_d$, when the bus voltage is U_d, while under three-level modulation, only the duty ratio of T_1 and T_2 is the same, but the 180 degrees phase difference exists, making the U_{AB} switched among U_d, 0 and $-U_d$.

For the time constant $\tau \gg T$, we can use simplified line (actually should be exponential curve) to describe the current change in modulation cycle, as in Figure 4, where U_{on} and U_D are the conduction voltage drop of switch tube and freewheeling diode, respectively.

i_{MAX} and i_{MIN} in Figure 4 are the maximum and minimum current in steady state. With the definitions of average current i_0, modulation period T and the ripple current Δi, we can have

$$\begin{cases} U_d = L\dfrac{di_{AB}(t)}{dt} + Ri_{AB} + 2U_{on} & 0 \leq t < t_1 \\ -U_d = L\dfrac{di_{AB}(t)}{dt} + Ri_{AB} + 2U_D & t_1 \leq t < T \end{cases} \quad (3)$$

From Figure 4, $i_{AB}(0) = i_{AB}(T) = i_{MIN}$, $i_{AB}(t_1) = i_{MAX}$, one can write

$$i_{MAX} = \left[\frac{U_d - 2U_{on}}{r} \cdot \left(1 - e^{-\frac{t_1}{\tau}}\right) + \frac{U_d + 2U_D}{r} \cdot \left(e^{-\frac{T}{\tau}} - e^{-\frac{t_1}{\tau}}\right)\right] \Big/ \quad (4)$$

$$\left(1 - e^{-\frac{T}{\tau}}\right),$$

$$i_{MIN} = \left[\frac{U_d - 2U_{on}}{r} \cdot \left(e^{-\frac{T-t_1}{\tau}} - e^{-\frac{T}{\tau}}\right) + \frac{U_d + 2U_D}{r} \cdot \left(e^{-\frac{T-t_1}{\tau}} - 1\right)\right] \Big/ \quad (5)$$

$$\left(1 - e^{-\frac{T}{\tau}}\right).$$

For time constant $\tau \gg T$, we simplify formulas (4) and (5) using Taylor series as

$$1 - e^{-k} = 1 - 1 + k - \frac{1}{2!}k^2 + \cdots \approx k. \quad (6)$$

Combining formulas (4)–(6), one can write

$$i_0 = \frac{i_{\text{MIN}} + i_{\text{MAX}}}{2}$$
$$= \frac{(U_d - 2U_{on})t_1 - (U_d + 2U_D)(T - t_1)}{rT}. \quad (7)$$

And,

$$t_1 = \frac{U_d + 2U_D + i_0 r}{2(U_d + U_D - U_{on})} \cdot T. \quad (8)$$

The ripple current is

$$\Delta i = i_{\text{MAX}} - i_{\text{MIN}}$$
$$= \frac{(T - t_1)t_1}{T} \cdot \frac{2(U_d + 2U_D - U_{on})}{L}. \quad (9)$$

By substituting (8) into (9), one can write

$$\Delta i = \frac{(U_d - 2U_{on} - i_0 r)(U_d + 2U_D + i_0 r)}{2(U + U_D - U_{on})f_s L}. \quad (10)$$

Ignoring the U_{on}, U_D and $i_0 r$, one can write

$$\Delta i \approx \frac{U_d}{2f_s L}, \quad (11)$$

where f_s is the modulation frequency.

Under three-level modulation, theoretically, the current in electromagnetic coil can maintain a constant value by constructing a return based on freewheeling diodes and power source, while the duty ratio of the PWM will be 50% as in Figure 5. However, with the resistor existing and leakage current in freewheeling loop, the current value will decrease slowly, as in Figure 6. Therefore, in a half-modulation period, T_1 and T_2 will be simultaneously enabled in a very short period of time (for example, 0–t_1) under feedback
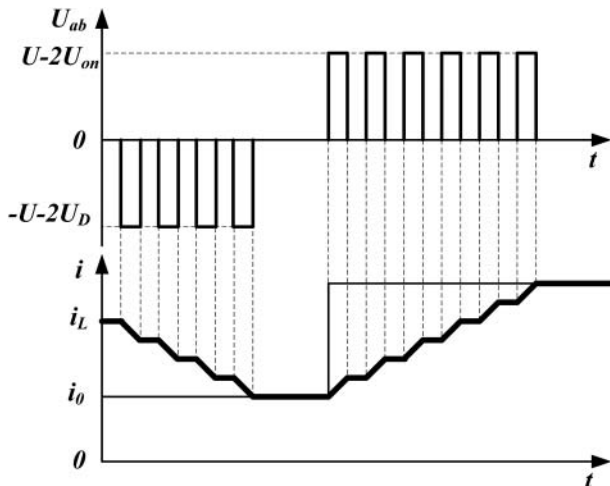

Figure 5. Voltage and current waveforms under three-level modulation in theory.
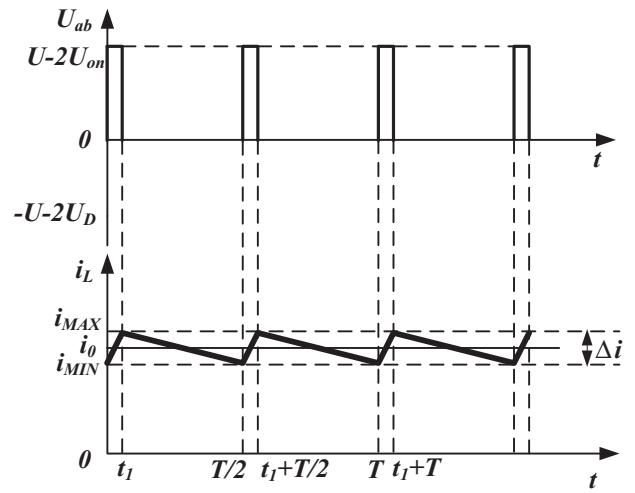

Figure 6. Voltage and current waveforms in tracking a constant current command under three-level modulation.

control, to maintain the average value of current as a constant when tracking a constant current command.

Similar with the two-level modulation, the current in electromagnetic coil can be expressed as

$$\begin{cases} U_d = L\frac{di_{AB}(t)}{dt} + Ri_{AB} + 2U_{on} & 0 \le t < t_1 \\ 0 = L\frac{di_{AB}(t)}{dt} + Ri_{AB} + U_{on} + U_D & t_1 \le t < T/2 \end{cases} \quad (12)$$

For $i_{AB}(0) = i_{AB}(T/2) = i_{\text{MIN}}$ and $i_{AB}(t_1) = i_{\text{MAX}}$,

$$i_{\text{MAX}} = \left[\frac{U_D + U_{on}}{r}\cdot\left(e^{-\frac{T/2}{\tau}} - e^{-\frac{t_1}{\tau}}\right) + \frac{U_d - 2U_{on}}{r}\cdot\left(1 - e^{-\frac{t_1}{\tau}}\right)\right] \Big/ \quad (13)$$
$$\left(1 - e^{-\frac{T/2}{\tau}}\right),$$

$$i_{\text{MIN}} = \left[\frac{U_D + U_{on}}{r}\cdot\left(e^{-\frac{T/2-t_1}{\tau}} - 1\right) + \frac{U_d - 2U_{on}}{r}\cdot\left(e^{-\frac{T/2-t_1}{\tau}} - e^{-\frac{T/2}{\tau}}\right)\right] \Big/ \quad (14)$$
$$\left(1 - e^{-\frac{T/2}{\tau}}\right).$$

For $\tau \gg T$, one can write

$$i_0 = \frac{i_{\text{MAX}} + i_{\text{MIN}}}{2}$$
$$= \frac{2(U_d - 2U_{on})t_1 - (U_D + U_{on})(T - 2t_1)}{rT}. \quad (15)$$

And,

$$t_1 = \frac{(U_D + U_{on} + i_0 r)}{(U_d + U_D - U_{on})} \cdot \frac{T}{2} \quad (16)$$

The ripple current is

$$\Delta i = i_{\text{MAX}} - i_{\text{MIN}}$$
$$= \frac{(T/2 - t_1)t_1}{T/2} \cdot \frac{(U_d + U_D - U_{on})}{L}. \quad (17)$$

By substituting (16) into (17), one can write

$$\Delta i = \frac{(U_{on} + U_D + i_0 r)(U_d - 2U_{on} - i_0 r)}{2(U_d + U_D - U_{on})f_s L}. \quad (18)$$

For U_d is much bigger than U_{on}, U_D and $i_0 r$, one can write

$$\Delta i \approx \frac{U_{on} + U_D + i_0 r}{2f_s L}. \quad (19)$$

From formulas (11) and (19), it can be known that the inherent ripple characteristic originates from the current fluctuation in the modulation period, influenced by the factors such as coil constant, bus voltage, modulation frequency, and topology mainly.

3.2. Errors in current detection circuit

As in Figure 7, by using current sensor and sampling resistor, the current in electromagnetic coil has been sampled and then outputted to the ADC (analog-digital converter) after filtering, bias and gain adjustment.

As in formula (20), G_t is the current sensor attenuation ratio, R_{sense} is the precise sampling resistor, G_{op} is the total gain of the amplifier circuit, and V_c is the output of current detection.

$$V_c = I_{AB} \frac{1}{G_t} R_{sense} G_{op}. \quad (20)$$

The following factors will cause the losses of precision: (1) noise and drift in circuit will cause the current ripple Δi and offset I_b. (2) G_t, R_{sense} and G_{op} will cause the gain error of detection circuit. (3) ADC has quantization error and nonlinear error.

3.2.1. Noise and drift in analog circuit

Analog noise is derived from the irregular movement of internal carrier of the device. Noise in the circuit is usually composed of various noise types, and it is difficult to separate the impacts of different types of noise. Usually, the noise model in the analog circuit is established by using the noise of voltage and current. The total noise output is the sum of the root mean square of each noise amplitude. For the circuit with resistor and amplifier, the total noise is the superposition of
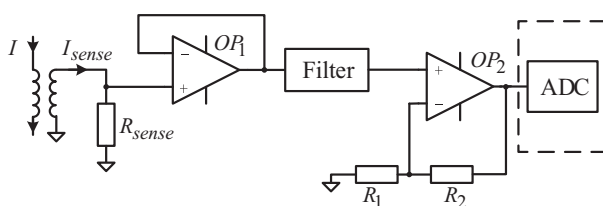

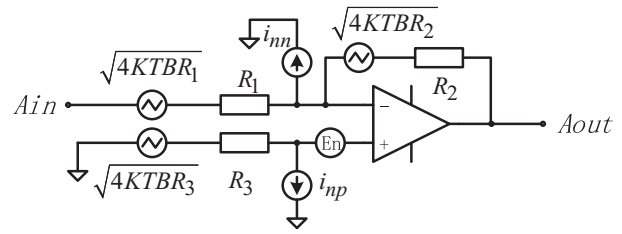**Figure 7.** Current detection circuit in DSPA.

Figure 8. Noise model of basic operational amplifier circuit.

thermal noise of resistor and the noises of amplifier voltage and current.

$$Vn^2 = 4KT \times R \times B. \quad (21)$$

The resistor thermal noise voltage is shown in formula (21), where K is the Boltzmann constant, T is the absolute temperature, and B is the frequency bandwidth (Hz). Thermal noise power and thermal noise voltage are as formulas (22) and (23), respectively.

$$Pn = \frac{Vn^2}{R} = 4KTB, \quad (22)$$

$$Vn = \sqrt{4KTRB}. \quad (23)$$

Figure 8 illustrates the noise model of basic operational amplifier circuit. E_n is the voltage noise connected to the positive input, while i_{np} and i_{nn} are the current sources connected to positive and negative input, respectively, to describe the current noises.

Formulas (24) and (25) describe the thermal noises and noise of operational amplifier, respectively, and we can have the total noise in formula (26).

$$E_{R\_rms} = \sqrt{\left[4KTR_1 \left(\frac{R_2}{R_1}\right)^2 + 4KTR_2 + 4KTR_3 \left(1 + \frac{R_2}{R_1}\right)^2 \right]B}, \quad (24)$$

$$E_{OP\_rms} = \sqrt{\left[(i_{nn}R_2)^2 + \left(i_{np}R_3 \left(1 + \frac{R_2}{R_1}\right)\right)^2 + \left(E_n \left(1 + \frac{R_2}{R_1}\right)\right)^2 \right]B}, \quad (25)$$

$$E_{Trms} = \sqrt{E_{OP\_rms}^2 + E_{R\_rms}^2}. \quad (26)$$

Drift in analog circuit mainly comes from the impedance matching failure and operational amplifier offset. The former can be solved by impedance isolation, while the latter model is shown in Figure 9. The final noise and drift in the multistage amplifier circuit will be amplified and accumulated step by step because of these gains at all levels.

Due to the asymmetry of the differential input of operational amplifier, offset voltage V_{io} and static bias current i_{bp} and i_{bn} will cause the inherent output
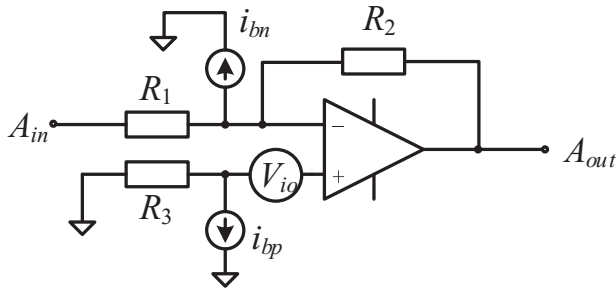
Figure 9. The i_{bn} and i_{bp} in drift model of the basic operational amplifier circuit.

Figure 10. Input and output characteristic of ADC.

offset, as in formula (27), where usually $R_3 = R_1 // R_2$, and i_{io} is the current offset caused by unbalanced static current.

$$V_{os} = \left(1 + \frac{R_2}{R_1}\right) V_{io} + i_{io} R_2. \tag{27}$$

Besides, common mode voltage and voltage fluctuation of the power will cause the other offsets, as ΔV_{CM} and ΔV_S in formula (28). The above two effects are added to the conventional offset voltage V_{iocon} by the CMRR (common-mode rejection ratio) and PSRR (power supply rejection ratio).

$$V_{io} = V_{iocon} + \frac{\Delta V_{CM}}{\text{CMRR}} + \frac{\Delta V_S}{\text{PSRR}}. \tag{28}$$

3.2.2. Error form ADC

The analog-to-digital conversion has two processes: (1) sampling process, the discrete sampling of the analog signal; (2) quantization process, means digital expression of analog signal.

There are quantization error and nonlinear error. The former is the main error, which decreases with the resolution of ADC device increasing; the latter is caused by factors such as offset error, gain error, integral linear error, differential linear error, temperature drift, and so on. High-resolution devices can be selected to meet the application requirements; furthermore, calibration can be carried out to improve the accuracy. The ideal characteristics of ADC are shown in formula (29), and U_n is the input voltage to be sampled, U_{REF} is the reference voltage, a_x is the digital output of conversion.

$$U_n = U_{REF}(2^{-1}a_1 + 2^{-2}a_2 + \cdots + 2^{-n}a_n). \tag{29}$$

A first-order model is often used to describe the real ADC input and output characteristic, as in formula (30), where K is the gain, ΔU is the offset, as shown in Figure 10.

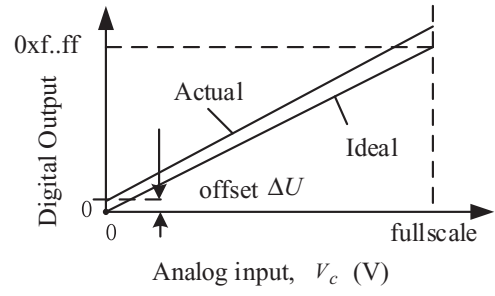$$U_n = KU_{REF}(2^{-1}a_1 + 2^{-2}a_2 + \cdots + 2^{-n}a_n) + \Delta U. \tag{30}$$

3.2.3. Calibration of whole current detection circuit

In formula (20), the inaccuracy of the resistors will cause the precision loss of R_{sense} and G_{op}, while current sensor will cause error in G_t. Furthermore, the magnetic flux leakage caused by magnetic core material and structure will lead to gain error and inherent drift.

By data fitting of the input and output data of current sensor, we can get a more accurate sensor model to correct the gain error and drift in current detection.

4. Experimental results and analysis

The experimental platform is shown in Figure 11. Power filter was designed to maintain the bus voltage stable and prevent switching noise transmitting into the power supply. A current control loop was designed based on DSP. Load was 4.528 mH, 1.6 Ω.

4.1. Noise and drift analysis

It is an effective way to adopt high-precision operational amplifiers to reduce the noise and drift in the circuit detection circuit. According to the circuit in Figure 6, the performance parameters of selected operational amplifiers are shown in Table 1.

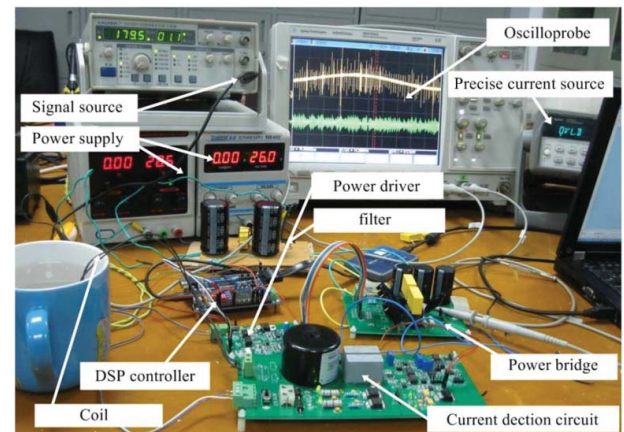From Table 1 and formula (31), $V_{os1} = V_{os2} = 10 \,\mu\text{V}$, the value of R_1 and R_2 are 2 kΩ, and the total

Figure 11. Experimental platform.

Table 1. Electrical characteristics of OPA2277.

Parameter	Condition	Typical value	Unit
Input offset voltage (V_{os})	–	±10	µV
Input offset voltage drift vs. temperature (dV_{os}/dt)	−40 to 85 °C	±0.1	µV/°C
Input offset voltage drift vs. time	−40 to 85 °C	0.2	µV/M
Input offset voltage drift vs. power supply (PSRR)	−40 to 85 °C	±0.1	µV/V
Input bias current (I_s)	–	±0.5	nA
Input offset current (I_{os})	–	±0.5	nA
Input voltage noise	–	0.22	µVpp
Input voltage noise density (E_n)	F < 10 kHz	8	nV/HZ
Current noise density	F = 1 kHz	0.2	pA/HZ
Common mode rejection (CMRR)	–	115	dB

voltage drift V_{os} in current detection circuit is 30 µV.

$$V_{os} = V_{os1} + \frac{R1 + R2}{R1} V_{os2}. \tag{31}$$

Design bandwidth of amplifier system is 2000 Hz. From Table 1, the current noise density is relatively small, and can be ignored. Therefore, the total noise in circuit is mainly caused by the voltage noise, and formulas (32) and (33) describe the noise of OP_1 and OP_2, respectively, in Figure 6. Formula (34) describes the thermal noise of a 2 kΩ resistor.

$$E_{op1} = \sqrt{fBDW} \times en \times Gop = 357.77 \, \text{nV}, \tag{32}$$

$$E_{op2} = \sqrt{fBDW} \times en \times Gop = 715.54 \, \text{nV}, \tag{33}$$

$$ER = \sqrt{4KTRB}$$
$$= \sqrt{4 \times 1.38 \times 10^{23} \times 298 \times 2000 \times 2000} \, \text{µV}$$
$$= 0.25 \, \text{µV}. \tag{34}$$

Total noise $ETrms$ of the current detection circuit can be approximated by formula (35),

$$ETrms = \sqrt{E_{op1}^2 + E_{op2}^2 + E_{R1}^2 + E_{R2}^2}$$
$$= 0.874 \, \text{µV}. \tag{35}$$

Setting the range of actual current sampling circuit as 0–10 V, the output current of the PA will be 0–10 A accordingly, with the coefficient is 1 A/V. So 30 µV drift and 0.874 µV noise in current detecting circuit will cause 30 µA drift and 0.874 µA ripple of current ripple, which are small enough obviously (less than 1% of the inherent ripple characteristic at vast majority of cases).

4.2. Calibration of ADC

According to formula (30), the calibration circuit in Figure 12 is designed to fit the sampling results of
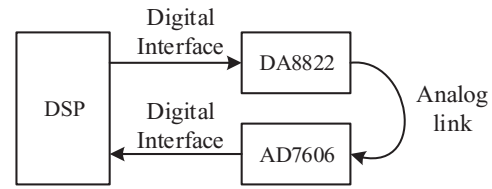
Figure 12. Calibration of analog-digital converter.
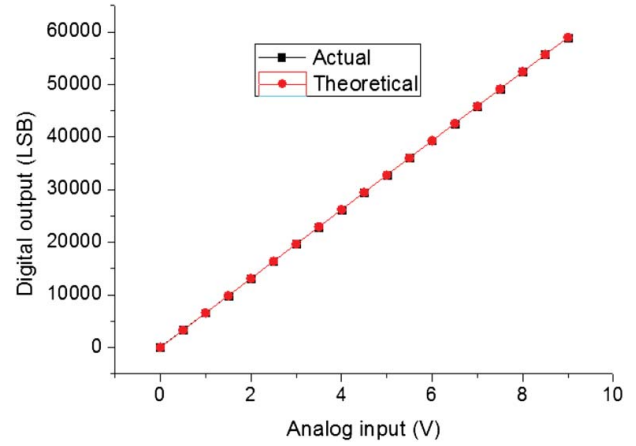
Figure 13. AD input–output characteristic after calibration.
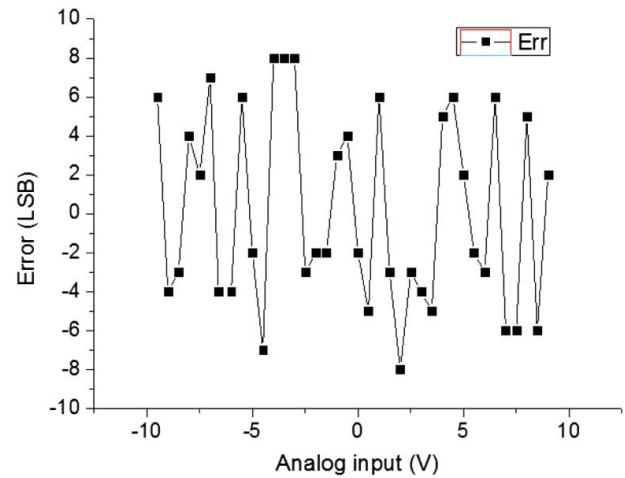
Figure 14. Error distribution after calibration.

ADC, considering that the DAC is easy to output high-precision analog signal.

The actual calibration equation is

$$D_{out} = 0.994 \times D_{in} + 10, \tag{36}$$

where D_{in} is the digital output of the ADC, and D_{out} is the result after calibration. As shown in Figure 13, the input–output characteristic is nearly ideal all over the input range after calibration.

Error distribution between theoretical and actual values after calibration is shown in Figure 14. For the input range is 0–10 V range, and under 16-bit resolution, the error is around ±8 LSB, leading to the actual
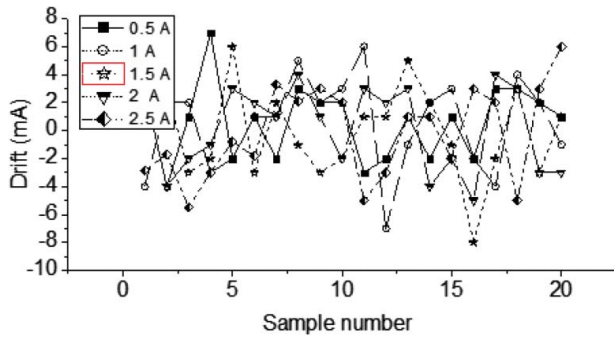
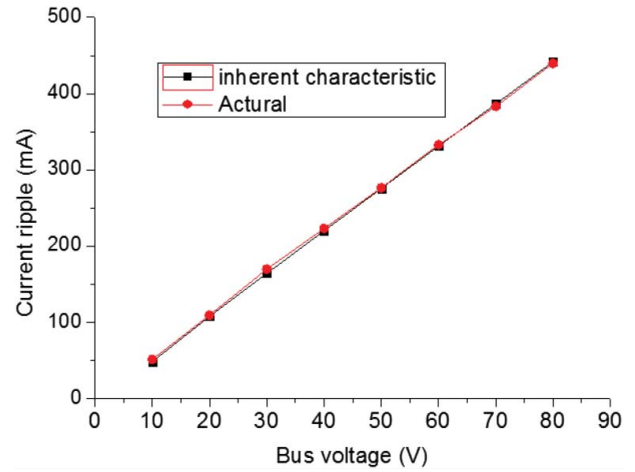**Figure 15.** Drift under different conditions.

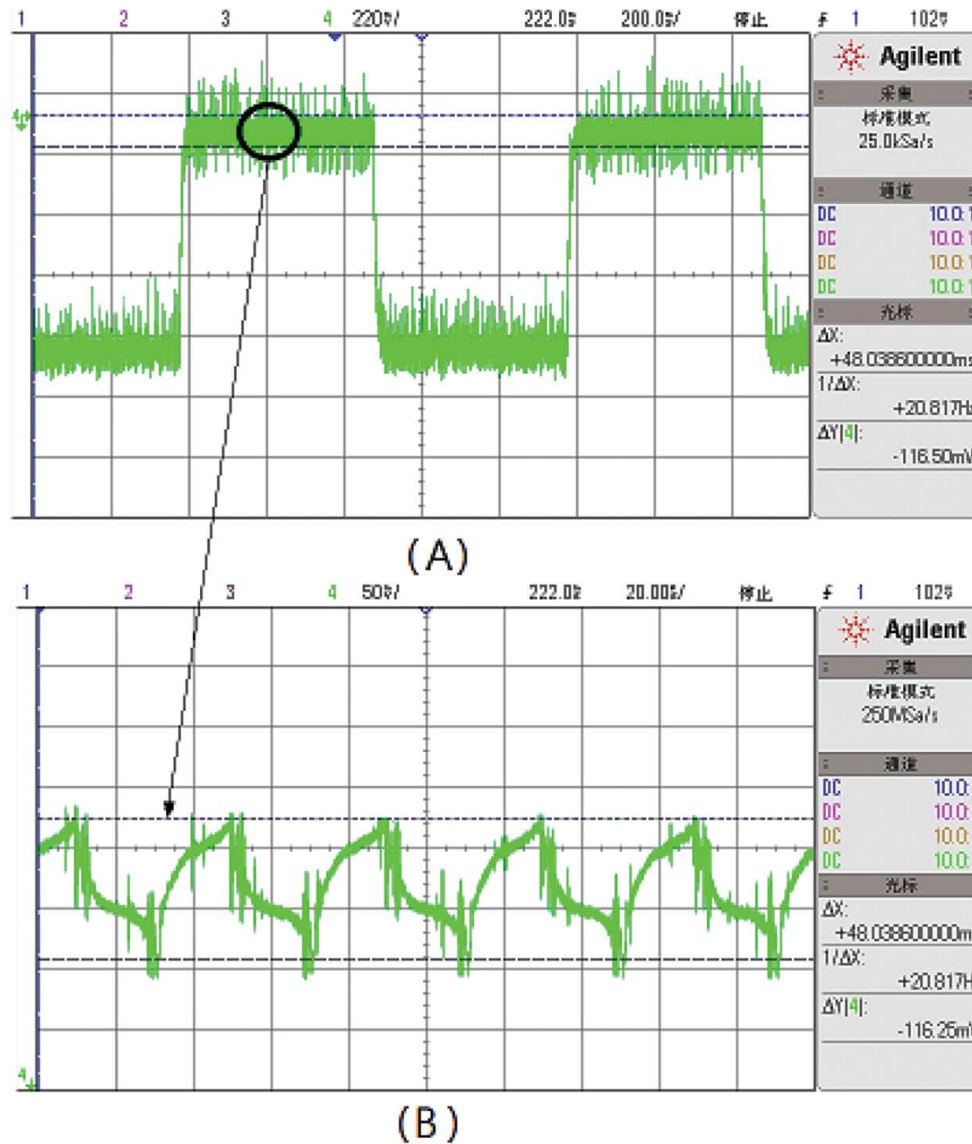**Figure 16.** Output current ripple at different bus voltage.

Figure 17. Ripple current waveforms in tracking a step command. Measured by oscilloscope: (A) 200 ms/div, (B) 20 μs/div. Bus voltage is 20 V, and modulation frequency is 20,000 Hz.

resolution of 1.2 mV, corresponding to 1.2 mA current detection accuracy.

4.3. Precision test under different conditions

The drift under different conditions is shown in Figure 15, with the bus voltage of 80 V and modulation frequency of 20 kHz. The drift is below 10 mA, with no obvious change under different output current condition.

To test the ripple performance, by setting modulation frequency as 20,000 Hz, we compared the values of theoretical inherent current ripple and average actual ripple, as shown in Figure 16 under different bus voltage. Furthermore, the error between actual output current ripple and inherent characteristic is shown in Figure 19.

Figures 17 and 18 illustrate the actual ripple current waveforms measured by oscilloscope in tracking a step command. We can measure the values of actual ripple current, and then compare with theoretical calculation of inherent characteristic in formula (11) as in Figures 16 and 19–21.

Then, considering the performance under difference modulation frequency, we set the bus voltage as 50 V, and compared the values of theoretical inherent current ripple and average actual ripple, as shown in Figure 20, with the corresponding error shown in Figure 21.

Once the magnetic coil of the magnetic bearing is selected, it means the fixed coil constant. On the whole, it seems that there is no obvious change of this error when the bus voltage and modulation frequency change, which means the inherent characteristic is
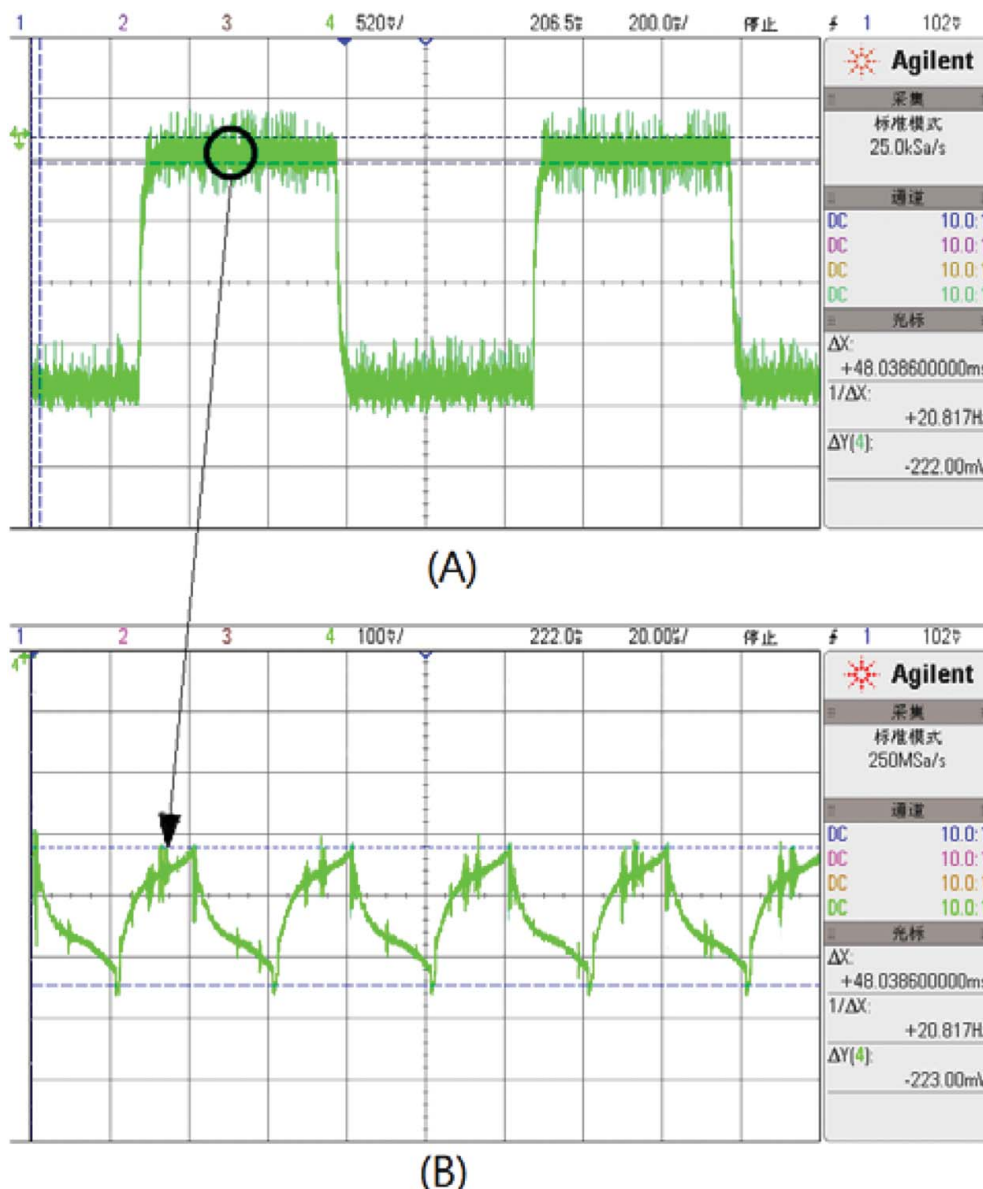

Figure 18. Ripple current waveforms in tracking a step command. Measured by oscilloscope: (A) 200 ms/div, (B) 20 μs/div. Bus voltage is 40 V, and modulation frequency is 20,000 Hz.
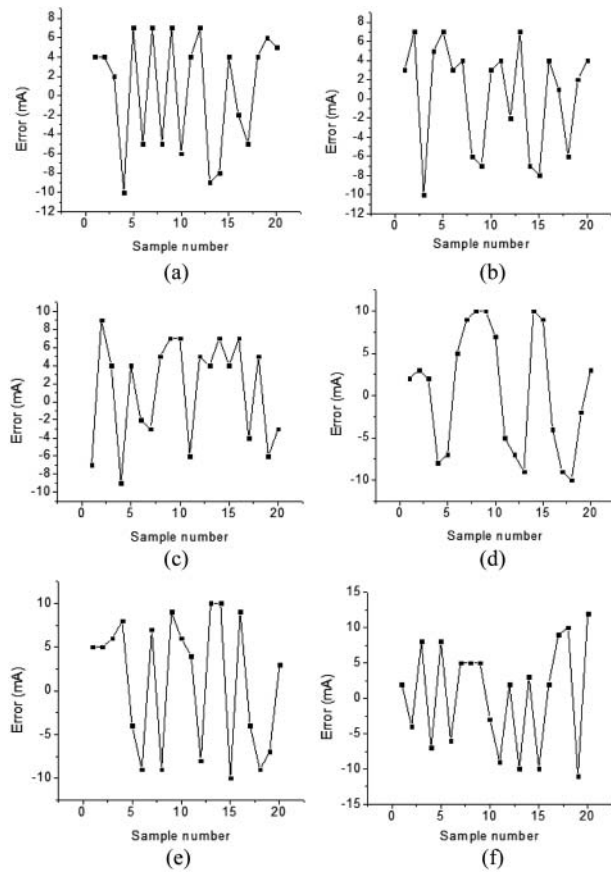
Figure 19. Error between the actual output current ripple and the inherent characteristic value when bus voltage is (a) 30 V, (b) 40 V, (c) 50 V, (d) 60 V, (e) 70 V, and (f) 80 V.
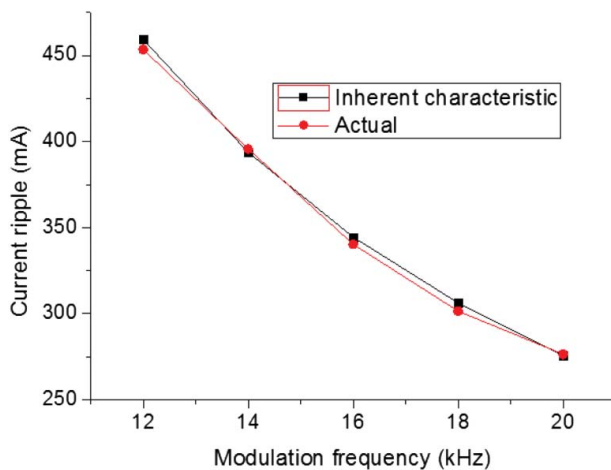

Figure 20. Output current ripple at different modulation frequency.
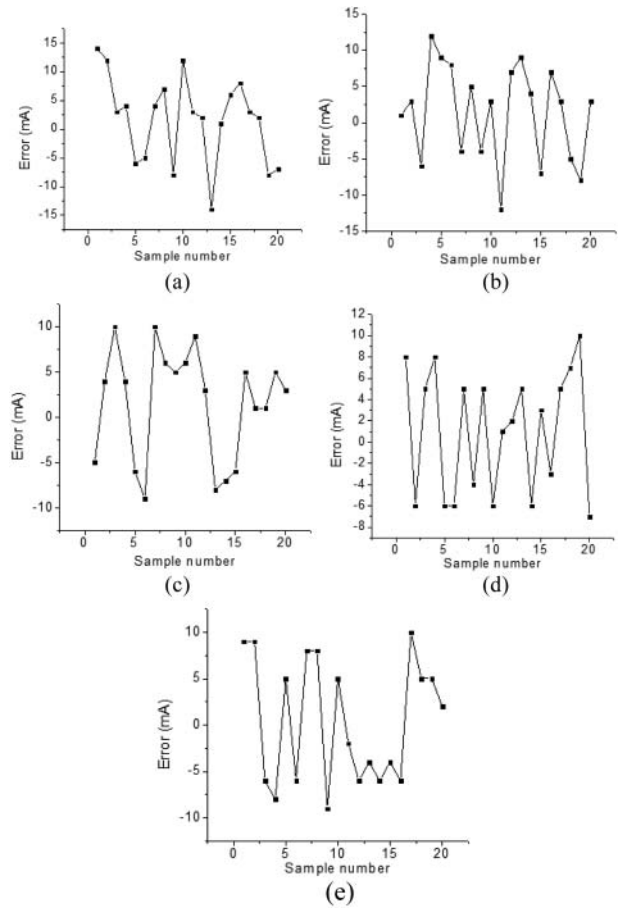

Figure 21. Error between the actual output current ripple and the inherent characteristic value when modulation frequency is (a) 12 kHz, (b) 14 kHz, (c) 16 kHz, (d) 18 kHz, and (e) 20 kHz.

characteristic, and will be influenced by factors such as inherent ripple characteristic and noise and drift in current detection circuit.

(2) Inherent ripple characteristic of DSPA is determined by bus voltage, modulation mode, modulation frequency and the constant of coil, as shown in formula (4), which is the decisive factor of realization of output precision.

(3) By suppressing the analog noise and drift, and improving the precision of current detection circuit, the approaches discussed can describe the formation of precision characteristics by theoretical calculation of inherent ripple characteristic even under different bus voltage and modulation frequency.

reliable to express the precision characteristics under the approaches discussed in this paper if the other factors, such as sampling precision, noise and drift, and the calibration of current detection circuit solved well.

5. Conclusion

(1) Precision characteristics of DSPA can be expressed through the output ripple and drift

Disclosure statement

No potential conflict of interest was reported by the authors.

Funding

References

[1] Tu X, Zhou R, Zhou Y, et al. Dynamical decoupling and feed-forward control for magnetically levitated planar actuators. Int J Appl Electromagnet Mech. 2017;54(1):57–76.

[2] Cheng X, Zeng H, Wu H, et al. Mathematical model and control implementation of switching power amplifier in magnetical-leviated system. J Huazhong Univ Sci Technol (Natl Sci Ed). 2015;43:493–496.

[3] Tu X, Zhou R, Zhou Y, et al. Measurement of initial phase for movers in magnetically levitated planer actuators. Int J Appl Electromagnet Mech. 2015;49(1):91–104.

[4] Zhou R, Zhou Y, Liu G, et al. Analysis of the eddy force disturbance on foil-wound coils in magnetic levitated planar motion. Int J Appl Electromagnet Mech. 2014;46(1):299–312.

[5] Cheng X. Data interchange mechanism in multi-axis ultra-precise synchronous motion control system. J Mech Eng. 2014;50(17):149–156.

[6] Cheng X, Zhou Y. Design of parallel computing architecture for multi-axis ultra-precise synchronous motion control. China Mech Eng. 2011;22(19):2156–2162.

[7] Mu H, Zhou Y, Wen X, et al. Calibration and compensation of cogging effect in a permanent magnet linear motor. Mechatronics. 2009;19(4):577–585.

[8] Zhu Y, Zhang S, Mu H. Augmentation of propulsion based on coil array commutation for magnetically levitated stage. IEEE Trans Magn. 2012;48(1):31–37.

[9] Ren Y, Fang J. Current-sensing resistor design to include current derivative in PWM H-Bridge unipolar switching power amplifiers for magnetic bearings. IEEE Trans Ind Electron. 2012;59(12):4590–4600.

[10] Mohamed YI, EI-Saadany E. An improved deadbeat current control scheme with a novel adaptive self-tuning load model for a three-phase PWM voltage-source inverter. IEEE Trans Ind Electron. 2007;54(2):747–759.

[11] Wen P, Lu TW. Decoupling control of a twin rotor MIMO system using robust deadbeat control technique. IET Control Theory Appl. 2008;2(11):999–1007.

[12] Mollov S, Babuska R, Abonyi J, et al. Effective optimization for fuzzy model predictive control. IEEE Trans Fuzzy Syst. 2004;12(5):661–675.

[13] Kouro S, Cortes P, Vargas R, et al. Model predictive control - a simple and powerful method to control power converters. IEEE Trans Ind Electron. 2009;56(6):1826–1838.

[14] Kempf C, Messner W, Tomizuka M, et al. Comparison of four discrete-time repetitive control algorithms. IEEE Control Syst. 1993;13(6):48–54.

[15] Bojoi RJ, Limongi LR, Roiu D, et al. Enhanced power quality control strategy for single-phase inverters in distributed generation systems. IEEE Trans Power Electron. 2011;26(3):798–806.

[16] Cheng X, Chen Q, Zeng H, et al. Reconfiguration rules for loosely-coupled redundant supporting structure in radial magnetic bearings. Int J Appl Electrom Mech. 2016;51(2):91–106.

[17] Cheng X, Liu H, Song S, et al. Reconfiguration of tightly-coupled redundant supporting structure in active magnetic bearings under the failures of electromagnetic actuators. 2017;54(3):421–432.

[18] Zeng XM, Xu LX, Liu ZX. Electrical control system of five degrees of freedom AMB principal axis for grinder. J Nanjing Univ Aeronaut Astronaut. 2001;33(6):560–564.

[19] Wang J, Xu LX. Equivalent mathematical models of switching power amplifier for magnetic bearing. Trans China Electro-tech Soc. 2010;25(4):53–59.

[20] Chang SH, Chen PY, Ting YH, et al. Robust current control-based sliding mode control with simple uncertainties estimation in permanent magnet synchronous motor drive systems. IET J Mag. 2011;47(1):58–74.